










In-depth Hirschfeld Surface Analysis, Interaction Energy, Molecular Docking, and DFT Investigations of Electronic Properties of 2,4-dimethyl-1-nitrobenzene

Youcef Megrouss*^{1,2} , Salem Yahiaoui^{2,3} , Nouridine Boukabcha^{1,2} ,
 Mansour Azayez¹ , Sid Ahmed Kaas⁴ , Abdelkader Chouaih² ,
 Mokhtaria Drissi^{2,5} 

¹ Chemistry Department, Faculty of Exact Sciences and Informatic, Hassiba Benbouali University, Chlef 02000, Algeria.

² Laboratory of Technology and Solid Properties (LTPS), Abdelhamid Ibn Badis University of Mostaganem, BP 227, Mostaganem, 27000, Algeria

³ Higher Normal School, Mostaganem 27000, Algeria.

⁴ Department of material science, faculty of science and technology, Tissemsilt University Algeria.

⁵ Laboratory of synthesis and catalyze, University IbnKhaldoun of Tiaret, 14000 Tiaret, Algeria

Abstract: Quantum-chemical calculations, molecular docking, and Hirshfeld surface analysis of a structure of 2,4-dimethyl-1-nitrobenzene constitute the main aspects of this work. The crystal structure of the title compound which is liquid at room temperature, was obtained by in situ cryo crystallization. The crystal packing is stabilized by C5–H5···O2 and C7–H7C···N1 intermolecular hydrogen bonds. The analysis of the obtained results of the density functional theory calculations is in good agreement with the experimental data. The analysis of global chemical reactivity descriptors shows that the compound exhibits more stability and less reactivity at high polar media. Hirshfeld surface and 2D-fingerprint plots analysis shows that the H...H, O...H/H...O, C...C, and C...H/H...C contacts are the significant contributors stabilizing the crystal structure of 2,4-dimethyl-1-nitrobenzene. The RDG-NCI analysis of the molecule was performed to determine the non-covalent interactions present within the molecule. In addition, the compound under investigation presents a biological activity when it is docked into the protein (PDB ID: 4Y0S) with the binding energy system of -6.6 kcal/mol.

Keywords: Molecular docking, Hirschfeld surface analysis, DFT, RDG, Interaction energy, ELF, LOL analysis

Submitted: March 19, 2023. **Accepted:** December 12, 2023.

Cite this: Megrouss Y, Yahiaoui S, Boukabcha N, Azayez M, Kaas SA, Chouaih A, Drissi M. In-depth Hirschfeld surface analysis, interaction energy, molecular docking, and DFT investigations of electronic properties of 2,4-dimethyl-1-nitrobenzene. JOTCSA. 2024;11(2):491-508.

DOI: <https://doi.org/10.18596/jotcsa.1259444>

***Corresponding author.** E-mail: y.megrouss@univ-chlef.dz ,youcefmegrouss@gmail.com

1. INTRODUCTION

Nitrobenzene is an organic compound with the chemical formula $C_6H_5NO_2$. It comes in the form of colorless liquid or yellow crystals depending on the temperature. The structure of nitrobenzene has been subject to several modifications, of which the hydrogen atoms of

the benzene ring can be substituted either in the ortho, meta, or para position by electrophilic or nucleophilic groups (1). Nitrobenzene and its derivatives have a wide application in industry because they are versatile intermediates in organic synthesis such as the production of aniline and, the synthesis of dyes, pesticides, and rubbers (2-

4). Nitrobenzene can also be used as a solvent for cellulose ester (2) and as an organochlorine fungicide for control of various fungal diseases caused by *Rhizoctonia solani*, *Botrytis* spp., *Aspergillus* spp., *Penicillium* spp., and *Tilletia caries* (5-6). Nitrobenzene is extremely toxic in large quantities which has a great impact on the human body (4). Nitro derivatives of benzene always demonstrate excellent heat resistance and insensitivity, because of their well-known π - π stacking (7). In recent years, nitrobenzene and its derivatives have been the subject of many theoretical studies by quantum chemical calculations (8-12). These latter are very powerful tools to reveal the structure-performance relationship and to give information about the electronic and structural properties of these materials with acceptable accuracy (13-14). A complete report of structural, electronic, and intermolecular interactions of methylated derivatives of nitrobenzene is shown in this work through X-ray diffraction data analysis, quantum chemical calculations, and Hirshfeld surface analysis of 2,4-dimethyl-1-nitrobenzene. This compound is a deep yellow-green color clear liquid with having characteristic odor. The experimental section was carried out by using the X-ray diffraction method, the structure of the compound studied has been deposited in the CCDC database under the CCDC references: [1017641](#) where the theoretical study is provided using density functional theory (DFT) with traditional hybrid functional (B3LYP) to exhibit its reactivity and discuss their physical and chemical properties. The biological properties of 2,4-dimethyl-1-nitrobenzene were investigated, by predicting the relative orientation of this compound when bound with an active site of a host molecule (protein) to form a stable complex. Hirshfeld surface analysis and the associated two-dimensional fingerprint plots are performed to understand what types of interatomic contacts are responsible for the stability of the crystal structure. The intermolecular interaction energies were calculated to understand and quantify the intermolecular interactions in a crystal lattice which drive the organization of the crystal packing in materials. The topological analyses of the electron localization function (ELF) and the localized orbital locator (LOL) analyses are exhibited for covalent bond analysis as they highlight parts of the surface of the molecular structure that have a high potential for a possible pair of electrons to be located.

2. COMPUTATIONAL DETAILS, DOCKING PROCESS, AND HIRSHFELD SURFACE ANALYSIS

The molecular geometry of the studied compound was optimized using B3LYP exchange-correlation functional (15,16) implemented in the Gaussian 09 package (17), which consists of the Lee-Yang Parr correlation functional in conjunction with a hybrid exchange functional first proposed by Becke. It is known that the reaction mechanism for such molecules is directly linked to their electrostatic environment. So, Fukui functions and the molecular electrostatic potential were calculated at the same level of calculation to predict the reactive sites for the electrophilic or nucleophilic attack for the compound under investigation. The Hirshfeld surface analysis was performed using the Crystal Explorer 17.5 program (18), where intermolecular interaction was quantitatively investigated based on the two-dimensional fingerprint plots. The ELF, LOL, and topological analysis were modeled using the Multiwfn 3.7 package (19). Finally, Auto dock-vina software was utilized for the docking process of 2,4-dimethyl-1-nitrobenzene into the protein receptor (PDB ID: 4Y0S), with choosing the dimensions $52 \times 74 \times 46 \text{ \AA}^3$ as grid box sizes.

3. RESULTS AND DISCUSSION

3.1. Molecular Geometry

The geometric of 2,4-dimethyl-1-nitrobenzene is optimized at DFT/B3LYP level using 6-31G (d,p) as the basis set, which is compared by those obtained experimentally by X-ray diffraction. When the X-ray structure of 2,4-dimethyl-1-nitrobenzene is compared with its optimized counterparts, slight conformational discrepancies are observed between them (Figure 1). For example, the calculated C-C within rings, C-N, and N-O bonds lengths values are in the ranges 1.3852-1.409, 1.4714, and 1.2324-1.2328 \AA , agree with the correspondent experimental values ranging of 1.3697-1.3945, 1.4812, and 1.2074-1.2175 respectively. Whereas, the maximum deviations of valence angle values from theoretical and experimental data do not exceed 1.35° . We thus note that the experimental results and the theoretical calculations are in good agreement as reflected by low values of root mean square deviations (RMSD) (Table 1).

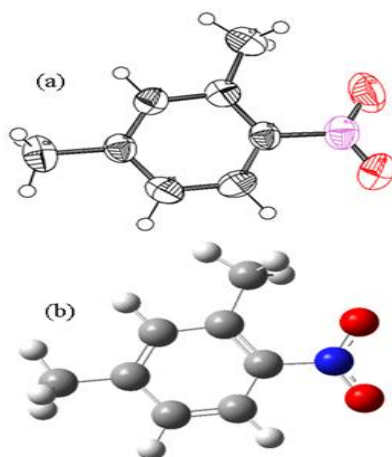


Figure 1: (a) Experimental structure and (b) optimized structure of 2,4-dimethyl-1-nitrobenzene.

3.2. Hirshfeld Surface Analysis and Intermolecular Contacts

The Hirshfeld surface analysis is a very efficient technique to quantify the intermolecular interactions among molecular crystals. Hirshfeld surfaces and the fingerprint plots illustrated in this work have been performed with the Crystal Explorer 17.5 (18). The distance of normalized contact (d_{norm}), is based on d_e and d_i and has been calculated by the following expression:

$$d_{norm} = \frac{d_i - r_i^{vdw}}{r_i^{vdw}} + \frac{d_e - r_e^{vdw}}{r_e^{vdw}}$$

where d_e is the distance from a point on the surface to the nearest nucleus outside the surface and d_i is defined as the distance from a point on the surface to the nearest nucleus inside the surface; with r_i^{vdw} present the van der Waals radius of the atom inside the Hirshfeld surface, whereas r_e^{vdw} corresponds to the van der Waals radius of the atom outside the Hirshfeld surface (20, 21).

The view of the three-dimensional Hirshfeld surface traced on d_{norm} in Figure 2 reveals two red dots, representing the contacts of the hydrogen with each oxygen atom of the nitro group. Hirshfeld surface analysis of the crystal along with d_{norm} , d_i , d_e , shape index, curvedness, and fragment patch is plotted in

Figure 3 and depicts the electron density interaction for the chosen compound with its neighboring molecule. From Figure 3, on the shape index map, we can see that the molecules are connected by π - π stacking interactions which are denoted by the adjacent red and blue triangles (highlighted by red circles), the triangles colored blue are convex areas that signify the existence of aromatic carbon atoms in the inside surface, whereas the red colored triangles signify concave areas due to the carbon atoms of the π -stacked molecule over it. The existence of the π - π clustering is distinctly seen in the curvedness surface. The wide green areas indicate a flat surface, and the blue areas exhibit curvature. Figure 4 displays the two-dimensional (2D) fingerprint plot that reflects the different intermolecular interaction contributions overlapping in the entire fingerprint and individual from each interaction. The highest significant numbers of interactions are the H...H interactions amounting to 47.5 %, because of a high quantity of hydrogen on the molecule surface. The second most important contribution was attributed to H...O/O...H interactions with 22.8%. other contributions may take place; these are fairly weak contacts C...C (7.8%), C...H/H...C (5.2%), N...C/C...N (3.5%), C...O/O...C (1.7%), N...H/H...N (1.2%), O...O (0.4%) illustrated in Figure 4.

Table 1: Bond distances and angles of atoms by X-ray and theoretical calculation.

Bond distances (Å)		X-ray	B3LYP/6-31G(d,p)	RMSD	
				0.055	
O1	N1	1.2074	1.2328		
O2	N1	1.2175	1.2324		
N1	C1	1.4812	1.4714		
C1	C2	1.3912	1.4090		
C1	C6	1.3806	1.3989		
C2	C3	1.3945	1.4032		
C2	C7	1.5025	1.5089		
C3	H3	0.9494	1.0867		
C3	C4	1.3851	1.3970		
C4	C5	1.3869	1.4027		
C4	C8	1.5113	1.5083		
C5	H5	0.9498	1.0862		
C5	C6	1.3697	1.3852		
Bond angles (°)				0.673	
O1	N1	O2	122.65	123.62	
O1	N1	C1	119.28	118.57	
O2	N1	C1	118.06	117.81	
N1	C1	C2	121.09	122.08	
N1	C1	C6	116.69	116.09	
C2	C1	C6	122.21	121.83	
C1	C2	C3	115.27	115.95	
C1	C2	C7	127.00	125.65	
C3	C2	C7	117.72	118.39	
C2	C3	C4	124.14	123.61	
C3	C4	C5	117.67	118.20	
C3	C4	C8	120.90	121.10	
C5	C4	C8	121.43	120.59	
C4	C5	C6	120.43	120.27	
C1	C6	C5	120.27	120.14	
Torsion (°)				3.65	
O1	N1	C1	C2	0.05	6.67
O1	N1	C1	C6	179.63	-173.35
O2	N1	C1	C2	179.29	-173.53
O2	N1	C1	C6	-1.03	6.44
N1	C1	C2	C3	179.37	179.98
C6	C1	C2	C7	-179.80	-179.58
N1	C1	C6	C5	179.78	179.73
C2	C1	C6	C5	0.11	-0.29
C1	C2	C3	C4	-1.26	0.31
C7	C2	C3	C4	179.44	179.93
C2	C3	C4	C8	179.71	179.56

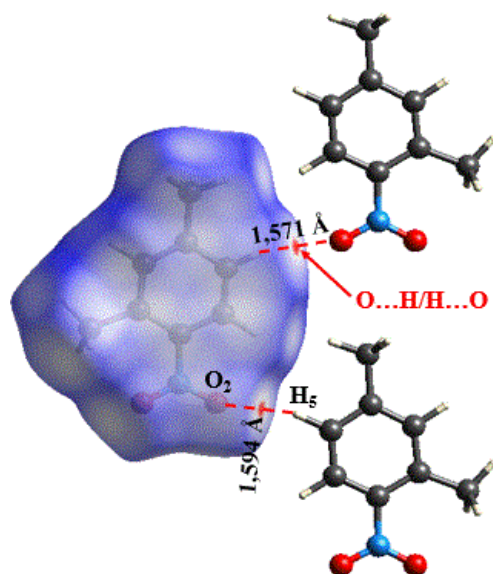


Figure 2: The view of the three-dimensional Hirshfeld surface plotted over d_{norm} .

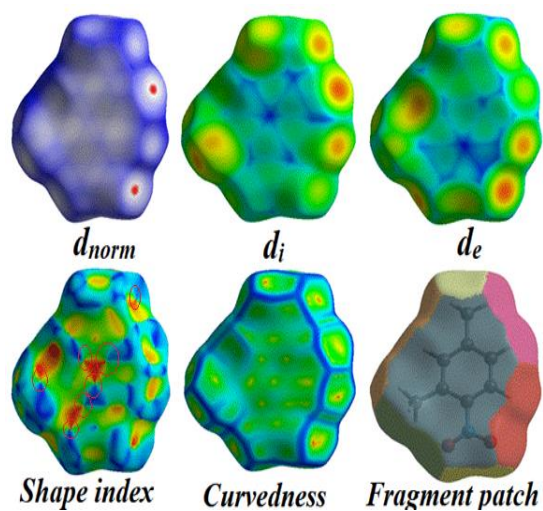


Figure 3: Hirshfeld surface analysis of the compound with d_{norm} , d_i , d_e , shape index, curvedness, and fragment patch.

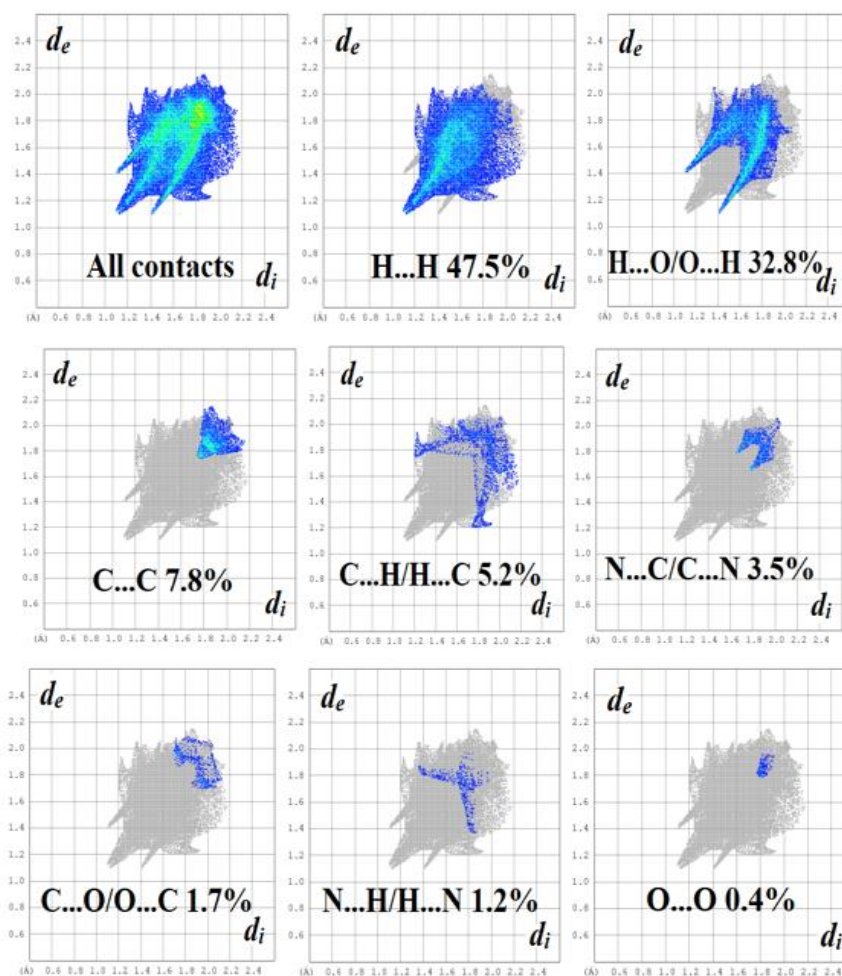


Figure 4: The 2D- Fingerprint plots showing the overall contribution to the total HS area and the individual percentages of the diverse intermolecular contacts of the molecule.

3.3. Interaction Energy and 3D energy frameworks

To understand and quantify the intermolecular interactions in a crystal lattice, including repulsion, electrostatics, dispersion, and polarization interactions energy, which occur and drives the organization of the crystal packing, the interaction energy was evaluated with the method CE-B3LYP/6-31G(d,p); energy model available in Crystal Explorer 17.5 software. The energy framework concept is a computational graphical tool for representing the magnitudes of interaction energies within

the crystal packing. Full interaction energy has been calculated by generating a cluster radius of 3.8 Å around the molecule. The energy framework represents the coulomb energy (in red tube), dispersion energy (green tube), and total energy (blue tube) (Figure 5). The energies have been calculated using a method for scaling different energy frameworks, indicating that the scaling factors for electrostatics, dispersion, polarization, and repulsion are 1.057, 0.740, 0.871, and 0.618, respectively (22).

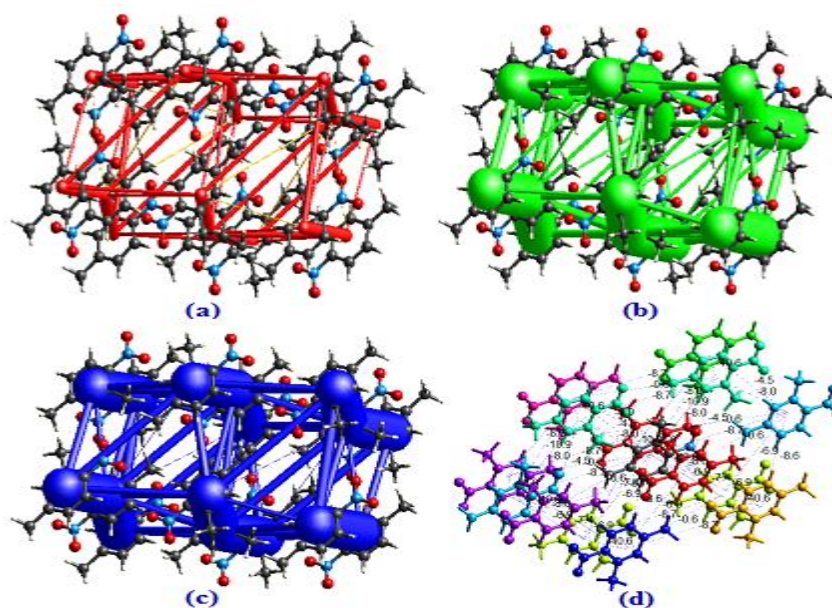


Figure 5: Energy frameworks calculated for 2,4-dimethyl-1-nitrobenzene, showing the (a) Coulomb energy (b) dispersion force (c) total energy, and (d) total energy diagram.

Table 2 demonstrates the IE calculation results for the component molecule given by respective colors. Whereas the global energies of the intermolecular interactions possible in the crystal cluster are in the range [-0.6, -40.6]

kJ/mol. The overall interaction energies are electrostatic ($E_{ele} = -29.5$ kJ/mol), polarization ($E_{pol} = -9.7$ kJ/mol), dispersion ($E_{dis} = -105.5$ kJ/mol), repulsion ($E_{repl} = 54.7$ kJ/mol), total interaction energy ($E_{tot} = -96.2$ kJ/mol).

Table 2: Energy framework detail of molecular interaction energies with symmetry operations (symop) for the compound. (distances between molecular centroids (R) in Å, interaction energies in kJ/mol, and number of pair-wise fragments (N)).

	N	Symop	R	Electron Density	E_ele	E_pol	E_dis	E_rep	E_tot
	2	x, -y+1/2, z+1/2	3.52	B3LYP/6-31G(d,p)	-12.0	-1.5	-48.0	24.2	-40.6
	1	-x, -y, -z	7.42	B3LYP/6-31G(d,p)	-3.3	-1.2	-4.1	0.8	-7.4
	2	-x, y+1/2, -z+1/2	7.69	B3LYP/6-31G(d,p)	-2.6	-1.5	-8.4	6.9	-6.9
	1	-x, -y, -z	7.51	B3LYP/6-31G(d,p)	-6.2	-1.4	-7.4	4.9	-10.9
	2	-x, y+1/2, -z+1/2	7.62	B3LYP/6-31G(d,p)	-2.2	-1.2	-10.6	7.3	-8.0
	2	x, y, z	9.74	B3LYP/6-31G(d,p)	-4.7	-1.4	-4.5	1.9	-8.7
	1	-x, -y, -z	7.71	B3LYP/6-31G(d,p)	-0.9	-0.8	-12.1	5.6	-8.6
	2	x, -y+1/2, z+1/2	10.56	B3LYP/6-31G(d,p)	1.4	-0.2	-3.2	1.4	-0.6
	1	-x, -y, -z	7.80	B3LYP/6-31G(d,p)	1.0	-0.5	-7.2	1.7	-4.5

3.4. Topological Analysis of Electronic Density (AIM) and Noncovalent Interactions Reduced Density Gradient (NCI-RDG) Analysis

Topological analysis has been performed to investigate the weak interactions of various materials with a more comprehensive approach. The theory of atoms in molecules (AIM) is greatly taken into account to evaluate the electron density of binding critical points (BCP) as well as to identify the various forms of interactions present in a molecular system (23). The hydrogen bonding properties were determined according to topological parameters including electron density $\rho(r)$, lagrangian kinetic energy $G(r)$, laplacian electron density $\nabla^2\rho(r)$, hamiltonian energy $H(r)$, and potential energy density $V(r)$, all these parameters are measured by atomic unit. The geometrical optimized structure has been applied to obtain the critical intramolecular bonding points (BCP) inside the crystal structure. The molecular graph of bond critical points for the title compound is illustrated in Figure 6, and the results of the calculations have been processed using the Multiwfn software. The topological parameters of the hydrogen-bonded interaction for the molecule are listed in Table 3. The electron density $\rho(r)$ and the laplacian $\nabla^2\rho(r)$ are significant in determining the type of interactions. In general, the large values of the electron density $\rho(r)$ and its laplacian $\nabla^2\rho(r)$ demonstrate strong hydrogen interactions. Positive laplacian $\nabla^2\rho(r)$ values are associated with a weak charge in the

interatomic region, while the negative readings could indicate the expression of a strong covalent nature (24). In this study, the electron density value (ρ_{BCP}) was found to be 0.01645 au and the Laplacian value was 0.06793 au. To determine the stability of the molecular structure, molecular interactions are involved. These interactions were able to be detected by reduced density gradient (RDG) analysis, based on the analysis of non-covalent interactions (NCI) present in the system (25). The NCI-RDG analysis is illustrated in Figure 7. The reduced density gradient (RDG) is a basic number consisting of the density and its first derivative, which is given by the formula below (26):

$$RDG(r) = \frac{1}{2(3\pi^2)^{\frac{1}{3}}} \frac{|\nabla\rho(r)|}{\rho(r)^{\frac{4}{3}}}$$

From Figure 7, the interaction between the different components is situated by an isosurface RDG around their proper area; the red dots reflect the repulsive effect. The greatest steric repulsion effect within the crystal has been seen at the center of the aromatic rings related to the π - π stacking interactions. The mixed red and green color zone surrounding (H7A, O1) and (O2, H6) between the aromatic ring and the nitro group represents a repulsive zone. The result of the NCI-RDG of the compound is in good agreement with the results of the Hirshfeld surface analysis (HAS) and XRD-packing.

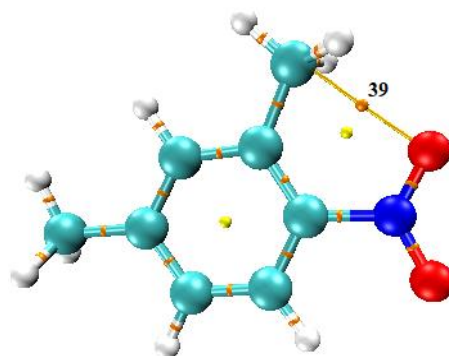


Figure 6: Molecular graph showing the bond critical point of the molecule.

Table 3. Topological parameters of hydrogen-bonded interaction for the title molecule.

Parameters	Ring critical point (RCP)
Electron density (ρ_{BCP}) (a.u)	0.01645
Laplacian of electron density (a.u)	0.06793
Lagrangian Kinetic Energy $G(r)$ (a.u)	0.01510
Hamiltonian Kinetic Energy $K(r)$ (a.u)	-0.00187
Potential energy density $V(r)$ (a.u)	-0.01322
Eigen Value λ_1	0.08624
Eigen Value λ_2	-0.1106
Eigen Value λ_3	-0.78841
H-Bond energy (kcal. Mol ⁻¹)	-0.00724

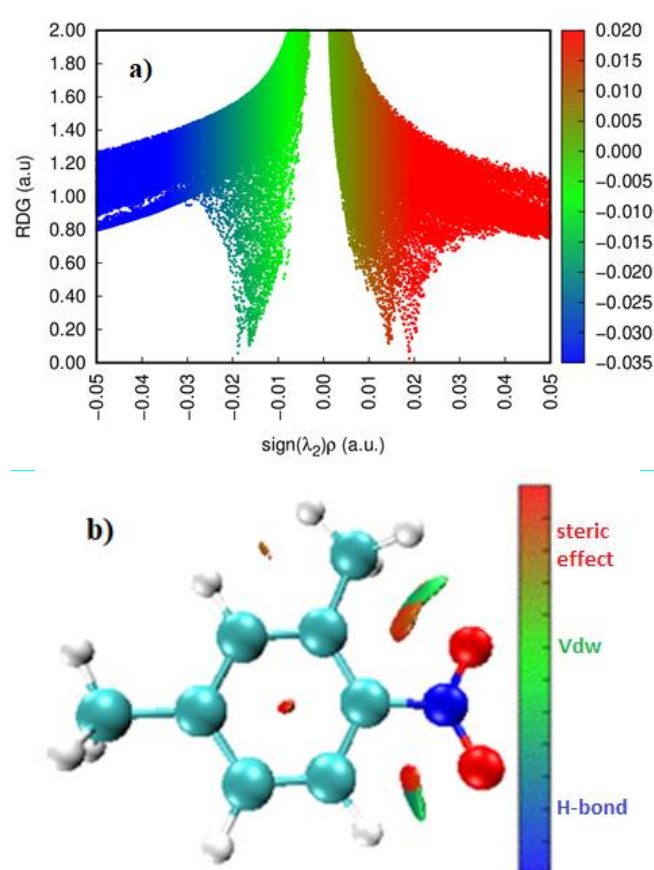


Figure 7: The scatter diagram (a) and the gradient isosurfaces (b) for the molecule.

3.5. ELF and LOL analysis

The topological analysis of the electron localization function (ELF) and the localized orbital locator (LOL) analysis are important methods for covalent bond analysis as they highlight parts of the surface of the molecular structure that have a high potential for a possible pair of electrons to be located. The ELF and LOL were modeled using the Multiwfn 3.7 package (19). ELF provides an understanding of the electron pair density and LOL provides an account of the maximum overlap of localized orbitals due to the orbitals gradient (27). The ELF chart is established within the interval 0.0 up to 1.0, although the area lower than 0.5 exhibits a delocalized electron region and the LOL achieves high values exceeding 0.5 in the areas of electron density localization dominance (28). The colors of the ELF and LOL maps shown in Figures 8 and 9 demonstrate the existence of binding and non-binding electrons,

with the red color surrounding the hydrogen atoms denoting the occurrence of both binding and non-binding electrons. High values of ELF or LOL shown in red surrounding hydrogen atoms are indicative of a strong electron localization caused by a covalent bond, a single electron pair, or a nucleus shell being present in that area. The color blue surrounding the carbon atoms of the dimethylbenzene group indicates the presence of a delocalized electron cloud. The two lone pairs of oxygen atoms are marked by weakly highlighted blue circles that mark less where the electrons are supposed to be delocalized. The region of hydrogen atoms has a relatively higher degree, which denotes the availability of localized bonding and non-bonding electrons. The middle zone in the hydrogen atom is white in the LOL because the electron density surpasses the maximum level of the color range.

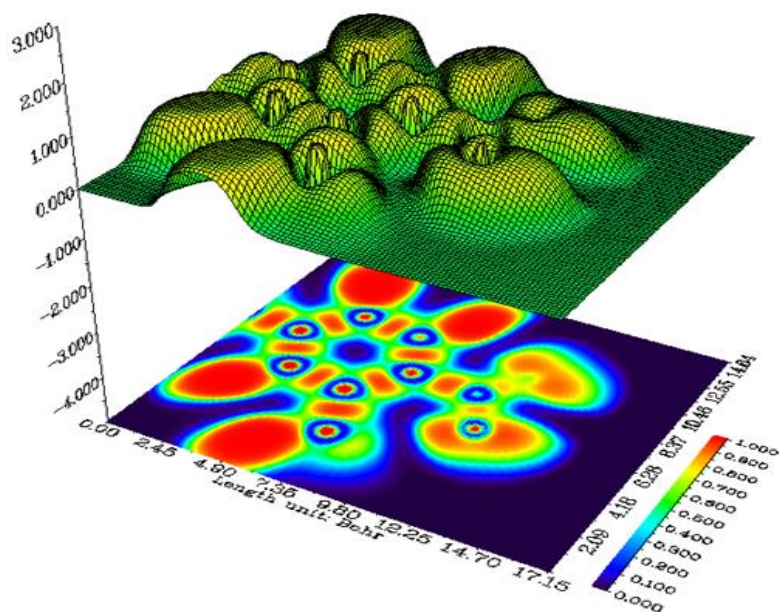


Figure 8: The relief map with a projection of ELF for the molecule.

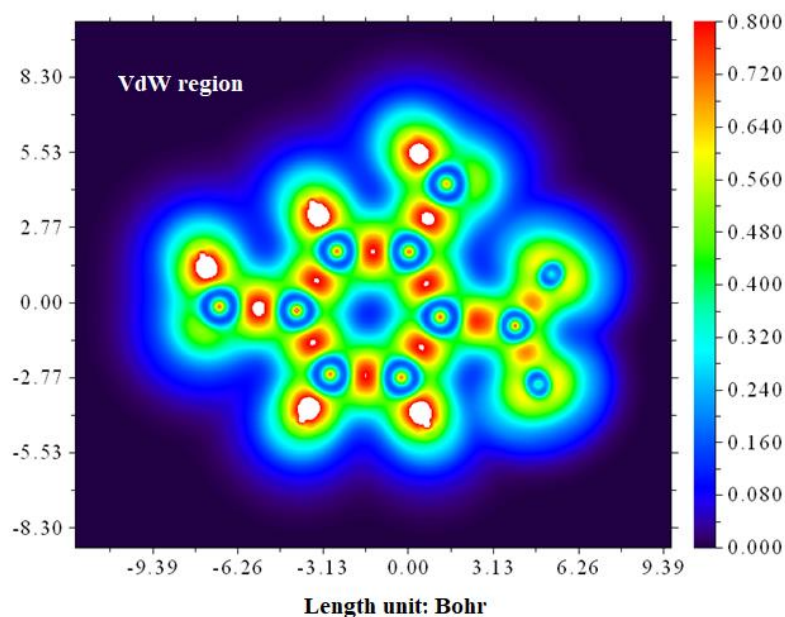


Figure 9: Contour LOL map of the molecule.

3.6. Frontier Molecular Orbitals, Global and Local Chemical Reactivity Descriptors Analysis

Molecular frontier orbitals provide a means of predicting the relative reactivity of a molecular system according to the electronic structure properties found in its structure. The molecular chemical properties in the molecule were controlled via its valence orbitals, thus nucleophilic attacks could be detected using the HOMO orbital, while the electrophilic attacks are checked through the LUMO orbital. The energy gap between HOMO (π donor) and LUMO (π acceptor) is taken as a measure of molecular structure stability (29). In the present research,

the HOMO as well as LUMO energies have been estimated using the Berny method (30-32) with a 6-31G(d,p) base set. Judging by the results given in Table 4, the gap energy between HOMO and LUMO is a critical parameter for the determination of the electrical transmission in the title molecule. The energy levels and allocations of the orbitals (HOMO \rightarrow LUMO) and (HOMO-1 \rightarrow LUMO+1) of the investigated molecule are depicted in Figure 10. Therefore, their molecular gap boundary values (ΔE_{gap}) were revealed to be 4.8 and 6.9245 eV in each case. The highest occupied molecular orbital (HOMO) is positioned above the nitro group which acts as an electron donor, whereas the

lowest unoccupied molecular orbital (LUMO) is located above the nitrobenzene.

Table 4: Energies of frontier orbitals of 2,4-dimethyl-1-nitrobenzene.

Energies (eV)	B3LYP /6-31G(d,p)
E_{HOMO}	-7.2466
E_{LUMO}	-2.4398
$E_{HOMO}-E_{LUMO}$ gap	4.80
E_{HOMO-1}	-7.3769
E_{LUMO+1}	-0.47
$E_{HOMO-1}-E_{LUMO+1}$ gap	6.9245

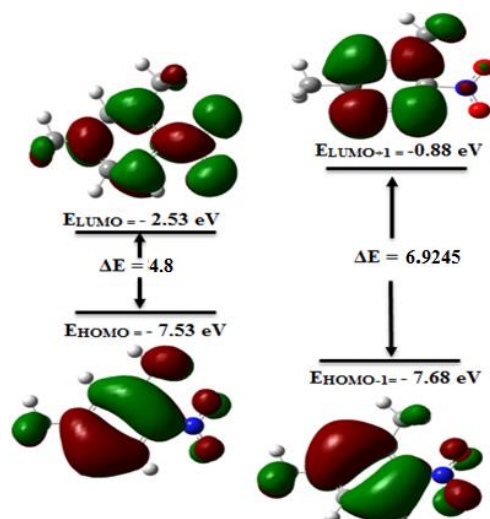


Figure 10: The frontier molecular orbitals for the molecule obtained by using the B3LYP method.

As it is well known, a high-value energy gap (ΔE) indicates that the molecular structure has higher kinetic stability, and a lower chemical reactivity (33). This approach is suitable to determine the properties of electrical transfer throughout the whole molecular structure. Thus, the values calculated of the global chemical reactivity descriptors, expressed below

(34-39), for 2,4-dimethyl-1-nitrobenzene are given in Table 5.

$$I = -E_{HOMO}; \eta = 1/2 (E_{LUMO} - E_{HOMO});$$

$$\eta = 1/2 (E_{LUMO} - E_{HOMO}); S = 1/2 \eta;$$

$$\mu = 1/2 (E_{LUMO} + E_{HOMO}); \omega = \frac{\mu^2}{2\eta};$$

$$\Gamma = E_{LUMO} - 2E_{HOMO} + E_{HOMO-1};$$

$$S^{(2)} = -\frac{\Gamma}{\eta^3}$$

Table 5: Global chemical reactivity descriptors of 2,4-dimethyl-1-nitrobenzene.

Parameters (eV)	DFT/B3LYP/6-31G(d,p)	
	In vacuum	In DMSO medium
Ionization potential (I)	7.246	6.93
Chemical hardness (η)	2.4	2.36
Chemical softness (s)	0.208	0.208
Chemical potential (μ)	-4.88	-4.57
Electrophilicity index (ω)	4.84	4.42
Hyper-hardness (Γ)	4.766	4.32
Hyper-softness ($S^{(2)}$)	-0.344	-0.328

A low value of ionization potential is observed in the DMSO medium indicating that this compound has the highest electron donor

character. The global chemical hardness values have increased and the global softness values have decreased in the presence of the high

polar solvent; 2,4-dimethyl-1-nitrobenzene exhibits less reactive properties with a low probability of intramolecular charge transfer in this medium. The value electrophilicity index in a vacuum medium is higher compared to that calculated in the gas state; this result indicates that this compound exhibits a low electrophile character in the polar environment. To characterize the reactivity or stability, the hyperhardness descriptor (Γ) has already inserted. Therefore, the positive values of hyperhardness in both media (4.766 and 4.32 eV) point to quite that the compound is stable and less reactive.

The local reactivity descriptor like the Fukui function indicates the preferred regions where a chemical species will amend its density when the numbers of electrons are modified or it indicates the tendency of the electronic density to deform at a given position upon accepting or donating electrons (40). Using NBO analysis of the neutral, cation, and anion state of the molecule, Fukui Functions are calculated using the following relations:

$$f_k^+ = [q(N+1) - q(N)] \text{ for nucleophilic attack}$$

$$f_k^- = [q(N) - q(N-1)] \text{ for electrophilic attack}$$

Where N, N-1, and N+1 are total electrons present in the neutral, cation, and anion states of the molecule, respectively.

In addition to these functions, local softness (s_k^+ , s_k^-) and local electrophilicity indices (ω_k^+ , ω_k^-) are also used to describe the reactivity of atoms in molecules. The local softness condensed to an atom location defined by (41):

$$s_k^+ = S f_k^+, \quad s_k^- = S f_k^-$$

and local electrophilicity indices (42) defined by

$$\omega_k^+ = \omega f_k^+, \quad \omega_k^- = \omega f_k^-$$

In the histogram shown in Figures 11 and 12 of the title compound, the relatively high value of local reactivity descriptors (f_k^+ , ω_k^+ , s_k^+) at C₅, C₁, and O₂ indicates that these sites are more prone to nucleophilic attack whereas the relative values of local reactivity descriptors (f_k^- , ω_k^- , s_k^-) at N indicate that this site is more prone to electrophilic attack.

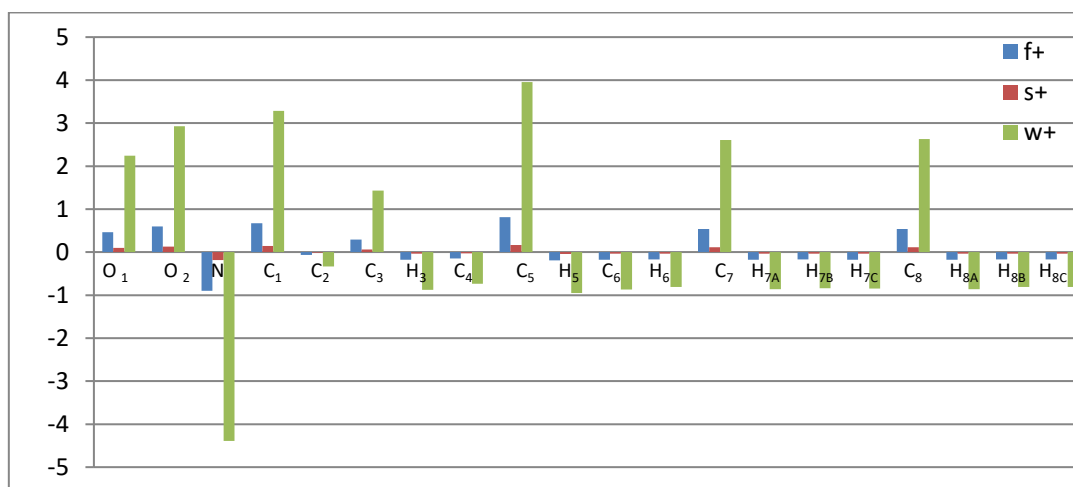


Figure 11: Local reactivity descriptors (f_k^+ , ω_k^+ , s_k^+) in eV for atomic sites of the molecule using NBO population analysis at B3LYP/6-31G(d,p) level.

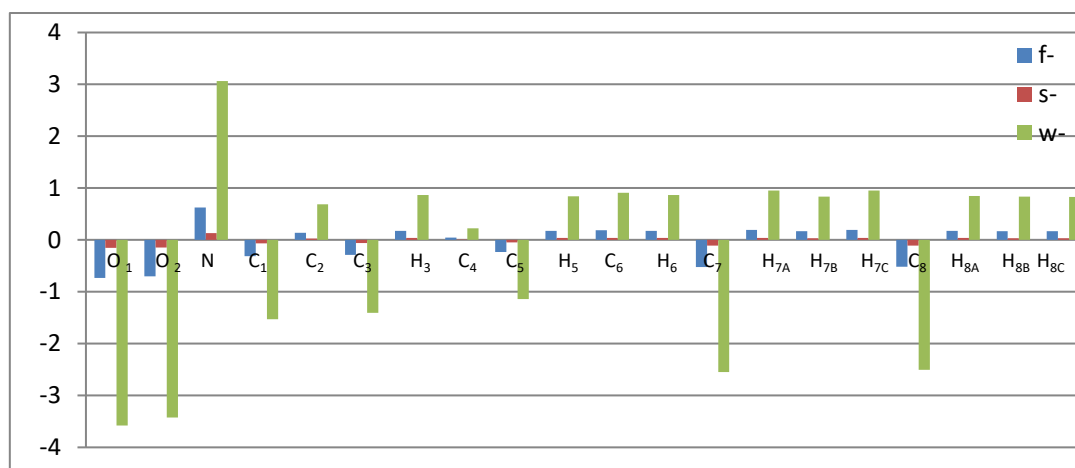


Figure 12: Local reactivity descriptors (f_k^- , ω_k^- , s_k^-) in eV for atomic sites of the molecule using NBO population analysis at B3LYP/6-31G(d,p) level.

3.7. Molecular Electrostatic Potential Analysis

An analysis of the molecular electrostatic potential surface (MEPS) has been affected to validate the evidence about the reactivity of 2,4-dimethyl-1-nitrobenzene. The MEPS can therefore provide information on the sign of different molecular regions. Colors red and blue in MEPS represent the most electron-rich

regions and those poor in electrons respectively. The compared x-ray and the DFT results led to an estimation of a similar electrostatic potential around the molecule (Figure 13). It thus was observed that the region is negative around the nitro groups (NO_2); the favored site for electrophilic attack, while for the blue zones, around the methyl group, nucleophilic attacks are taking place.

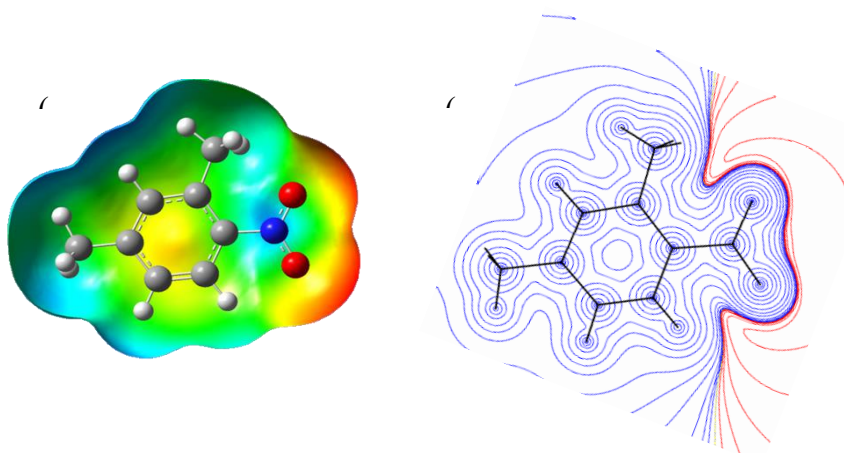


Figure 13: Electrostatic potential maps around the molecule. Panel (a) shows the DFT calculation of the electrostatic potential distribution, and panel (b) displays the electrostatic potential distribution predicted from the experimental X-ray diffraction data

3.8. Pass Analysis And Molecular Docking Studies

3.8.1. PASS analysis

The PASS tool allows us to explore the possible biological properties of compounds, based on their chemical formula. The potential biological properties of the selected compounds were investigated through the PASS web server (43). It uses 2D molecular fragments known as multilevel atom neighbor descriptors that suggest the biological activity of a chemical

compound based on its molecular structure. It gives the prediction score for biological properties on the ratio of probability to be active (P_a) and probability to be inactive (P_i). A higher P_a means the compound possesses more probability for the biological property (44). The exploration of biological activities of the selected compounds through the PASS analysis resulted in similar kinds of biological activities, the title compound was found to have great potential for biological activity as an Antibiotic Glycopeptide-like, with P_a ranging from 0,937

to 0,734 when $P_a > P_i$. The probability of the biological activities of our compound is collected in Table 6. The title compound could have a potential inhibitory effect against beta-lactoglobulin binding protein, in the current study. This protein was chosen based on the high P_a value ($P_a = 0.937$). The crystal structure of this target protein (PDB ID: 4Y0S) was obtained from the protein data bank (45). β -lactoglobulin (LG) is a protein belonging to the lipocalin family (46).

Lipocalins are often involved in the binding, storage, and transport of low-molecular-weight hydrophobic ligands (47). The ability to bind small molecules has made lipocalins an interesting target for utilization as a new class of drug transporters (48). Several proteins from this family have been modified and engineered to bind molecular targets with high specificity and selectivity (49,50).

Table 6: PASS prediction for the activity spectrum of the title compound. P_a represents the probability to be active and P_i represents the probability to be inactive.

PA	PI	Biological activity
0.937	0.001	Antibiotic Glycopeptide-like
0.909	0.005	Ubiquinol-cytochrome-c reductase inhibitor
0.811	0.007	Glucan endo-1,6-beta-glucosidase inhibitor
0.795	0.021	Acrocyllindropepsin inhibitor
0.795	0.021	Chymosin inhibitor
0.795	0.021	Saccharopepsin inhibitor
0.760	0.049	Phobic disorders treatment
0.746	0.020	Acylcarnitine hydrolase inhibitor
0.746	0.007	Pterin deaminase inhibitor
0.734	0.004	Mannan endo-1,4-beta-mannosidase inhibitor

3.8.2. Molecular docking

Molecular docking is a method that predicts the relative orientation of one molecule (ligand) when bound with an active site of another molecule (protein) to form a stable complex such that the free energy of the overall system is minimized. In the current study, we can recognize the transfer of a molecule known as ligand 2,4-dimethyl-1-nitrobenzene in biological complex systems. Autodock-Vina software (51) was utilized and the title molecule was docked into the protein receptor (PDB ID: 4Y0S). The active site of the protein was determined with the following dimensions: grid box sizes: 52×74×46 Å; x, y, z centers: -3, 8, and 21 respectively. The ligand has a better docking ability to protein when its binding energy has a minimum value (52). The binding affinities and

their root-mean-square deviation (RMSD) values for different poses in 4Y0S inhibitors are reported in Table 7. Generally, the docked conformation with the lowest binding energy is selected as the best pose for molecular docking (53). From Table 7 it can be seen that the best docking pose was determined with the binding energy system (ligand-protein) of -6.6 kcal/mol in mode number 1. This value is lower compared to the binding energy of previous works, using the same target protein (PDB ID: 4Y0S) and the same active site. The docking results were visualized by Accelrys Discovery Studio (version 4.1) software, The lowest energy pose for the compound (2,4-dimethyl-1-nitrobenzene in the protein binding site was shown in Figure 14.

Table 7: Docking results of the binding affinity and RMSD values of different poses in 4Y0S inhibitor of the title compound.

mode	Affinity (Kcal/mol)	RMSD l.b	RMSD u.b.
1	-6.6	0.000	0.000
2	-6.3	1.845	2.577
3	-6.1	1.837	2.779
4	-5.4	2.544	3.416
5	-5.1	3.862	5.055
6	-4.8	3.390	4.413
7	-4.6	6.934	8.379
8	-4.4	5.077	6.427
9	-4.4	6.989	8.243

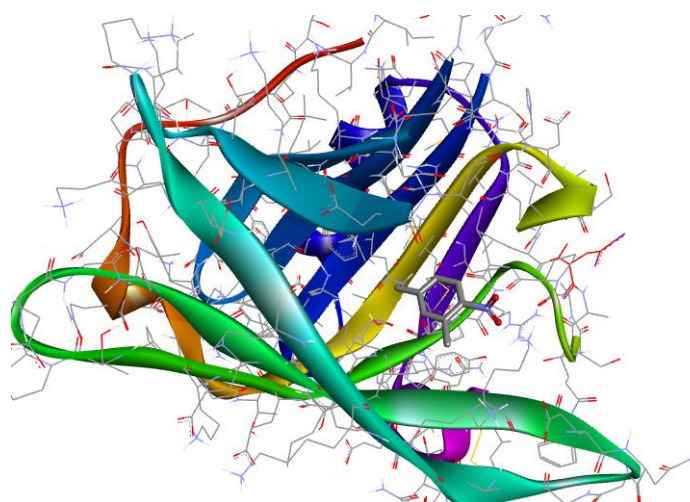


Figure 14: Best-scored docking pose of the title compound inside active sites of the 4Y0S protein.

The intermolecular interactions, linking the structure of our ligand and the 4Y0S protein, are represented in Figure 15 with two forms (form A: 2D and form B: 3D). On the other

hand, the types of intermolecular interactions existing between the residues of the 4Y0S protein and the ligand studied are illustrated in Table 8.

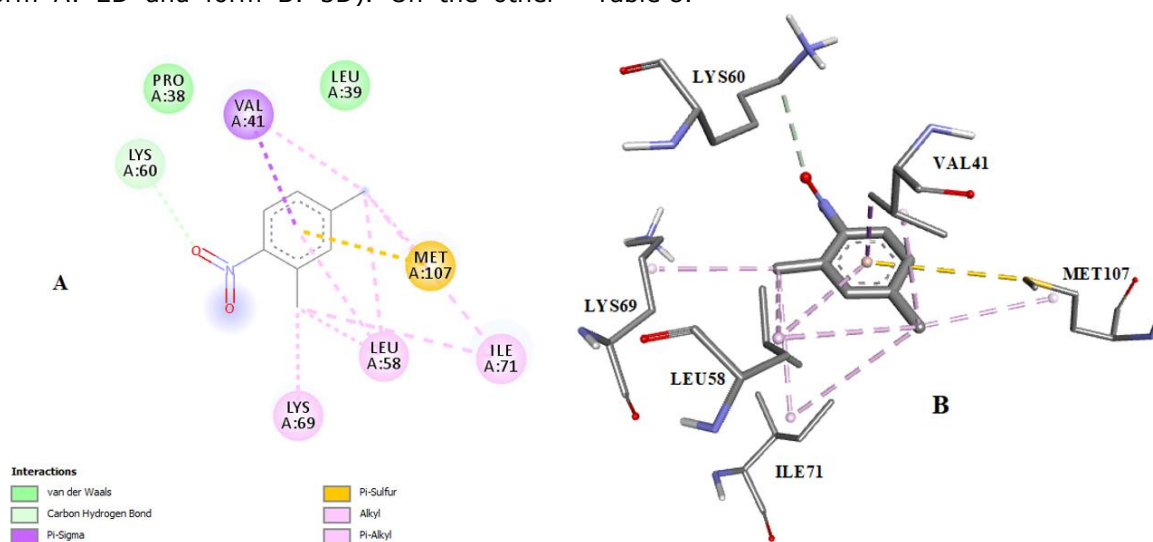


Figure 15: Two forms of intermolecular interactions, linking the structure of the ligand with the protein 1NTK (A 2D and B 3D).

Table 8: Distances, types, and location of intermolecular interactions formed from the residues of the protein C-met (PDB ID: 4Y0S) and the title molecule.

Protein	Residues	Compound	Atom/group of compound	Category	Types	Distance (Å)
PDB (ID : 4Y0S)	A:LYS60	2,4-dimethyl-1-nitrobenzene	O2	Hydrogen Bond	Carbon Hydrogen Bond	3.525
	A:VAL41		aromatic ring	Hydrophobic	Pi-Sigma	3.469
	A:MET107		aromatic ring	Miscellaneous	Pi-Sulfur	5.196
	A:LEU58		C8	Hydrophobic	Alkyl	5.027
	A:LEU58		aromatic ring	Hydrophobic	Pi-Alkyl	5.403
	A:LEU58		C7	Hydrophobic	Alkyl	4.579

A:LYS69	C7	Hydrophobic	Alkyl	4.146
A:ILE71	C8	Hydrophobic	Alkyl	5.313
A:ILE71	C7	Hydrophobic	Alkyl	4.909
A:MET107	C8	Hydrophobic	Alkyl	4.648

4. CONCLUSION

In the present work, DFT calculations, molecular docking, and Hirshfeld surface analysis of 2,4-dimethyl-1-nitrobenzene were reported. B3LYP function with 6-31G(d,p) basis set calculations of geometry optimization shows that the obtained theoretically optimized bond lengths and bond angles are in good agreement with the corresponding experimental ones. The variation of global chemical reactivity descriptors of E-TPDN in two media showed that this compound exhibits a high reactivity in the gaseous phase, while it exhibits a good electrophile character in a polar solvent such as DMSO medium. The general conclusion from the estimation of the electrostatic potential of the 2,4-dimethyl-1-nitrobenzene molecule in both experimental and theoretical studies is that the region of the nitro around the nitro group is a favored site for electrophilic attack while the methyl groups region is electropositive. The Hirshfeld surface analysis and the subsequent 2D-fingerprint plots have indicated that the crystal is principally stabilized by two types of interactions; H...H contacts with 47.5 % and H...O/O...H interactions with 22.8%. This study reveals that the title molecule has a significant hyperpolarizability and can be used to develop NLO materials. The RDG-NCI analysis of these molecules was performed to determine the non-covalent interactions present within the molecules. According to the results, we can say that the molecule is the most reactive. The title under investigation presents a biological activity (Antibiotic Glycopeptide-like), its ability of docking into the protein 4Y0S is confirmed with the binding energy system (ligand-protein) of -6.6 kcal/mol.

5. ACKNOWLEDGMENTS

We thank the Ministry of Higher Education and Scientific Research and the General Directorate of Scientific Research and Technological Development (DG-RSDT) for their support. We also thank the laboratory: Crystallography Laboratory, Department of Physics, Ondokuz Mayıs University, Samsun, TURKEY in which the data collection was carried out.

6. REFERENCES

1. Minasyan YV, Degtyarenko AI, Kosmacheva KD, Plekhovich SD, Zelentsov SV. Effect of Acceptor and Donor Substituents in The ortho, meta, and para Positions in the Nitrobenzene Molecule on the Reaction of Interaction with Ethylene. Multidisciplinary

Digital Publishing Institute Proceedings. 2018;9(1):50. Available from: [<URL>](#)

2. Program NT. Report on carcinogens, 2011. National Toxicology Program, US Department of Health and Human Services, Washington, DC. 2011.

3. Services UDoHaH. Hazardous substances data bank (HSDB, online database). National Toxicology Information Program, National Library of Medicine, Bethesda, MD. 1993. Available from: [<URL>](#)

4. Atsdr U. Agency for toxic substances and disease registry. Case Studies in environmental medicine <http://www.atsdr.cdc.gov/HEC/CSEM/csem.html>. 1997.

5. Arora PK, Sasikala C, Ramana CV. Degradation of chlorinated nitroaromatic compounds. Applied microbiology and biotechnology. 2012;93:2265-77. Available from: [<URL>](#)

6. Tas DO, Pavlostathis SG. Occurrence, toxicity, and biotransformation of pentachloronitrobenzene and chloroanilines. Critical Reviews in Environmental Science and Technology. 2014;44(5):473-518. Available from: [<URL>](#)

7. Zhang J, Mitchell LA, Parrish DA, Shreeve JnM. Enforced layer-by-layer stacking of energetic salts towards high-performance insensitive energetic materials. Journal of the American Chemical Society. 2015;137(33):10532-5. Available from: [<URL>](#)

8. Cardenuto MH, Champagne B. The first hyperpolarizability of nitrobenzene in benzene solutions: investigation of the effects of electron correlation within the sequential QM/MM approach. Physical Chemistry Chemical Physics. 2015;17(36):23634-42. Available from: [<URL>](#)

9. Soto J, Algarra M. Electronic structure of nitrobenzene: A benchmark example of the accuracy of the multi-state CASPT2 theory. The Journal of Physical Chemistry A. 2021;125(43):9431-7. Available from: [<URL>](#)

10. Millán R, Soriano MD, Cerdá Moreno C, Boronat M, Concepción P. Combined spectroscopic and computational study of nitrobenzene activation on non-noble metals-based mono- and bimetallic catalysts. Nanomaterials. 2021;11(8):2037. Available from: [<URL>](#)

11. Boubegra N, Megrouss Y, Boukabcha N, Chouaih A, Hamzaoui F. The electrostatic properties of 1, 2-dimethyl-3-nitrobenzene compound: ab initio calculation and X-ray charge density analysis. Rasayan Journal of Chemistry. 2016;9(4). Available from: [<URL>](#)

12. Kumar MS, Vibhanjali M, Tripathi P, Adil KM. Quantum Chemical Descriptors Based QSTR Study of Nitrobenzene Derivatives against Tetrahymena

Pyriformis. Research Journal of Chemical Sciences. ISSN.2231:606X. Available from: [<URL>](#)

13. Krishnakumar S, Das AK, Singh PJ, Shastri A, Rajasekhar B. Experimental and computational studies on the electronic excited states of nitrobenzene. *Journal of Quantitative Spectroscopy and Radiative Transfer*. 2016;184:89-99. Available from: [<URL>](#)

14. Seshadri S, Padmavathy M. Structure, characterization and DFT studies of 1, 2-Dichloro-4-fluoro-5-Nitrobenzene. 2018. Available from: [<URL>](#)

15. Lee C, Yang W, Parr RG. Development of the Colle-Salvetti correlation-energy formula into a functional of the electron density. *Physical review B*. 1988;37(2):785. Available from: [<URL>](#)

16. Becke AD. Density-functional exchange-energy approximation with correct asymptotic behavior. *Physical review A*. 1988;38(6):3098. Available from: [<URL>](#)

17. Caricato M, Frisch MJ, Hincsocks J. Gaussian 09: IOps Reference: Gaussian Wallingford, CT, USA; 2009. Available from: [<URL>](#)

18. Turner M, McKinnon J, Wolff S, Grimwood D, Spackman P, Jayatilaka D, et al. CrystalExplorer (Version 17.5). University of Western Australia. 2017.

19. Lu T, Chen F. Multiwfn: A multifunctional wavefunction analyzer. *Journal of computational chemistry*. 2012;33(5):580-92. Available from: [<URL>](#)

20. Kanmazalp SD, Macit M, Dege N. Hirshfeld surface, crystal structure and spectroscopic characterization of (E)-4-(diethylamino)-2-((4-phenoxyphenylimino) methyl) phenol with DFT studies. *Journal of Molecular Structure*. 2019;1179:181-91. Available from: [<URL>](#)

21. Kansız S, Dege N. Synthesis, crystallographic structure, DFT calculations and Hirshfeld surface analysis of a fumarate bridged Co (II) coordination polymer. *Journal of Molecular Structure*. 2018;1173:42-51. Available from: [<URL>](#)

22. Turner MJ, Grabowsky S, Jayatilaka D, Spackman MA. Accurate and efficient model energies for exploring intermolecular interactions in molecular crystals. *The journal of physical chemistry letters*. 2014;5(24):4249-55. Available from: [<URL>](#)

23. Bader R. A quantum theory. Clarendon: Oxford, UK. 1990.

24. Johnson ER, Keinan S, Mori-Sánchez P, Contreras-García J, Cohen AJ, Yang W. Revealing noncovalent interactions. *Journal of the American Chemical Society*. 2010;132(18):6498-506. Available from: [<URL>](#)

25. Aouad MR, Messali M, Rezki N, Said MA, Lentz D, Zubaydi L, et al. Hydrophobic pocket docking, double-proton prototropic tautomerism in contradiction to single-proton transfer in thione \rightleftharpoons thiol Schiff base with triazole-thione moiety: Green synthesis, XRD and DFT-analysis. *Journal of Molecular Structure*. 2019;1180:455-61. Available from: [<URL>](#)

26. Agarwal P, Bee S, Gupta A, Tandon P, Rastogi V, Mishra S, et al. Quantum chemical study on influence of intermolecular hydrogen bonding on the geometry, the atomic charges and the vibrational dynamics of 2, 6-dichlorobenzonitrile. *Spectrochimica Acta Part A: Molecular and Biomolecular Spectroscopy*. 2014;121:464-82. Available from: [<URL>](#)

27. Jacobsen H. Localized-orbital locator (LOL) profiles of chemical bonding. *Canadian Journal of Chemistry*. 2008;86(7):695-702. Available from: [<URL>](#)

28. Silvi B, Savin A. Classification of chemical bonds based on topological analysis of electron localization functions. *Nature*. 1994;371(6499):683-6. Available from: [<URL>](#)

29. Jensen F. Introduction to computational chemistry: John wiley & sons; 2017.

30. Cohen HD, Roothaan C. Electric dipole polarizability of atoms by the Hartree-Fock method. I. Theory for closed-shell systems. *The Journal of chemical physics*. 1965;43(10):S34-S9. Available from: [<URL>](#)

31. Demirtaş G, Dege N, İçbudak H, Yurdakul Ö, Büyükgüngör O. Experimental and DFT Studies on Poly [di- μ 3-acesulfamato-O, O: O'; O': O, O-di- μ -acesulfamato-O, O; N-di- μ -aqua-dicalcium (II)] Complex. *Journal of Inorganic and Organometallic Polymers and Materials*. 2012;22:671-9. Available from: [<URL>](#)

32. Evecen M, Tanak H, Tinmaz F, Dege N, İlhan İÖ. Experimental (XRD, IR and NMR) and theoretical investigations on 1-(2-nitrobenzoyl) 3, 5-bis (4-methoxyphenyl)-4, 5-dihydro-1H-pyrazole. *Journal of Molecular Structure*. 2016;1126:117-26. Available from: [<URL>](#)

33. Aihara J-i. Reduced HOMO-LUMO gap as an index of kinetic stability for polycyclic aromatic hydrocarbons. *The Journal of Physical Chemistry A*. 1999;103(37):7487-95. Available from: [<URL>](#)

34. Fuentealba P, Parr RG. Higher-order derivatives in density-functional theory, especially the hardness derivative $\eta/\partial N$. *The Journal of chemical physics*. 1991;94(8):5559-64. Available from: [<URL>](#)

35. Mulliken RS. A new electroaffinity scale; together with data on valence states and on valence ionization potentials and electron affinities. *The Journal of Chemical Physics*. 1934;2(11):782-93. Available from: [<URL>](#)

36. Pearson RG. Hard and soft acids and bases. *Journal of the American chemical society*. 1963;85(22):3533-9. Available from: [<URL>](#)

37. Pearson RG. Absolute electronegativity and hardness correlated with molecular orbital theory. *Proceedings of the National Academy of Sciences*. 1986;83(22):8440-1. Available from: [<URL>](#)

38. Chattaraj PK, Roy DR. Update 1 of: electrophilicity index. *Chemical reviews*. 2007;107(9):PR46-PR74. Available from: [<URL>](#)

39. Ayers PW, Parr RG. Beyond electronegativity and local hardness: Higher-order equalization criteria for determination of a ground-state electron density. *The Journal of chemical physics*. 2008;129(5). Available from: [<URL>](#)
40. Demircioğlu Z, Kaştaş ÇA, Büyükgüngör O. Theoretical analysis (NBO, NPA, Mulliken Population Method) and molecular orbital studies (hardness, chemical potential, electrophilicity and Fukui function analysis) of (E)-2-((4-hydroxy-2-methylphenylimino)methyl)-3-methoxyphenol. *Journal of Molecular structure*. 2015;1091:183-95. Available from: [<URL>](#)
41. Lee C, Yang W, Parr RG. Local softness and chemical reactivity in the molecules CO, SCN⁻ and H₂CO. *Journal of Molecular Structure: Theochem*. 1988;163:305-13. Available from: [<URL>](#)
42. Chattaraj PK, Maiti B, Sarkar U. Philicity: a unified treatment of chemical reactivity and selectivity. *The Journal of Physical Chemistry A*. 2003;107(25):4973-5. Available from: [<URL>](#)
43. Filimonov D, Lagunin A, Glorizova T, Rudik A, Druzhilovskii D, Pogodin P, et al. Prediction of the biological activity spectra of organic compounds using the PASS online web resource. *Chemistry of Heterocyclic Compounds*. 2014;50:444-57. Available from: [<URL>](#)
44. Thomas R, Hossain M, Mary YS, Resmi K, Armaković S, Armaković SJ, et al. Spectroscopic analysis and molecular docking of imidazole derivatives and investigation of its reactive properties by DFT and molecular dynamics simulations. *Journal of Molecular Structure*. 2018;1158:156-75. Available from: [<URL>](#)
45. Loch JI, Bonarek P, Polit A, Jablonski M, Czub M, Ye X, Lewinski, K. Goat beta-lactoglobulin complex with pramocaine (GLG-PRM) PDB May 25, 2020. Available from: [<URL>](#)
46. Sawyer L, Kontopidis G. The core lipocalin, bovine β -lactoglobulin. *Biochimica et Biophysica Acta (BBA)-Protein Structure and Molecular Enzymology*. 2000;1482(1-2):136-48. Available from: [<URL>](#)
47. Flower DR. The lipocalin protein family: structure and function. *Biochemical journal*. 1996;318(1):1-14. Available from: [<URL>](#)
48. Richter A, Eggenstein E, Skerra A. Anticalins: exploiting a non-Ig scaffold with hypervariable loops for the engineering of binding proteins. *FEBS letters*. 2014;588(2):213-8. Available from: [<URL>](#)
49. Gilbreth RN, Koide S. Structural insights for engineering binding proteins based on non-antibody scaffolds. *Current opinion in structural biology*. 2012;22(4):413-20. Available from: [<URL>](#)
50. Loch JI, Bonarek P, Polit A, Jabłoński M, Czub M, Ye X, et al. β -Lactoglobulin interactions with local anaesthetic drugs—Crystallographic and calorimetric studies. *International journal of biological macromolecules*. 2015;80:87-94. Available from: [<URL>](#)
51. Li H, Wang H-Y, Kang S, Silverman RB, Poulos TL. Electrostatic control of isoform selective inhibitor binding in nitric oxide synthase. *Biochemistry*. 2016;55(26):3702-7. Available from: [<URL>](#)
52. Mumit MA, Pal TK, Alam MA, Islam MA-A-A-A, Paul S, Sheikh MC. DFT studies on vibrational and electronic spectra, HOMO-LUMO, MEP, HOMA, NBO and molecular docking analysis of benzyl-3-N-(2, 4, 5-trimethoxyphenylmethylene) hydrazinecarbodithioate. *Journal of molecular structure*. 2020;1220:128715. Available from: [<URL>](#)
53. Guerroudj AR, Boukabcha N, Benmohammed A, Dege N, Belkafouf NEH, Khelloul N, et al. Synthesis, crystal structure, vibrational spectral investigation, intermolecular interactions, chemical reactivity, NLO properties and molecular docking analysis on (E)-N-(4-nitrobenzylidene)-3-chlorobenzenamine: A combined experimental and theoretical study. *Journal of Molecular Structure*. 2021;1240:130589. Available from: [<URL>](#)